International Journal of Engineering

Journal Homepage: www.ije.ir

Analysis of Aeolian Vibrations of Transmission Line Conductors and Extraction of Damper Optimal Placement with a Comprehensive Methodology

A. Rezaei*, M. H. Sadeghi

Department of Mechanical Engineering, University of Tabriz, Tabriz, Iran

PAPER INFO

Paper history:
Received 26 February 2018
Received in revised form 20 April 2018
Accepted 26 April 2018

Keywords:
Aeolian Vibration
Transmission Line
Energy Balance Method
Stock-bridge Damper
Optimum Location

ABSTRACT

Energy balance method is an effective and simple method which is used in the amplitude calculation of Aeolian vibration in transmission lines with Stockbridge damper. However, the accuracy of the results obtained by this method, heavily depends on the assumed mode shapes of the conductor vibration. In this study, by considering an appropriate model for the conductor vibration, a comprehensive methodology is presented to calculate the steady-state vibration amplitude of a conductor with arbitrary number of dampers. In this proposed method, the effects of traveling waves, variations of amplitude and phase, boundary conditions (finite length of the conductor), as well as the effect of number, location and impedance of the dampers are taken into account. Natural frequencies, damping rates and complex mode shapes are also obtained from forming and solving the nonlinear eigenvalue problem. Using this method, the effects of the damper placement on the vibration amplitude and bending strain are examined to achieve an optimum damper location. The comparison of the obtained values shows that considering the above parameters has a significant effect on the accuracy of the results.

***doi**: 10.5829/ije.2019.32.02b.19*

1. INTRODUCTION

In response to weather conditions, overhead conductors are moving with different characteristics. Aeolian vibration of power lines in windy climates lead to line failure as a result of material fatigue. Roots and consequences of this phenomenon are explained in many researches [1-5]. Wind-induced vibrations occur as a result of the very low internal damping of the conductors. So, to dissipate the wind energy and to reduce the conductor vibration amplitudes, different types of external dampers are used in the power line networks. One can find more information about various dampers like Stockbridge, Dog-bone, Spiral and etc. in literature [6]. Stockbridge damper is the most common damper that used to protect conductors of overhead transmission lines from aeolian vibrations [1, 7, 8]. This type of damper not only leads to energy dissipation because of the strand slippage of the damper cable, but also acts as a dynamic vibration absorber [8].

*Corresponding Author Email: *a.rezaei@tabrizu.ac.ir* (A. Rezaei)

The empirical study of the factors related to the conductor Aeolian vibration and its fatigue failure, started about a century ago [9]. However, the theoretical modeling of this phenomenon began in nearly half a century ago [10]. A number of researchers employed numerical methods for solving conductor vibration problems [11-13]. On the other hand, some other researchers adapted experimental results in conjunction with theoretical methods to evaluate the vibration state [14-16] and to predict the transmission lines fatigue life [17, 18]. From the practical view point, the Energy Balance Method (EBM/EBP) is a good and simple way to determine the maximum amplitude of the conductor vibration and it is widely used to reach this goal [19-23]. Steady-state vibration amplitude obtained by this method depends heavily upon the estimated energy dissipation amount which itself is calculated based on assumptions made about vibration mode shapes. In the classical procedure of EBM, the dissipated energy estimation is carried out by the assumption of standing harmonic wave in the entire span [14, 15]. The assumption of a standing wave is not correct in a non-

Please cite this article as: A. Rezaei, M. H. Sadeghi, Analysis of Aeolian Vibrations of Transmission Line Conductors and Extraction of Damper Optimal Placement with a Comprehensive Methodology, International Journal of Engineering (IJE), IJE TRANSACTIONS B: Applications Vol. 32, No. 2, (February 2019) 328-337

conservative system and it does not correctly reflect the effects of damper impedance and the energy travelling. To overcome these shortcomings, the response of the conductor vibration is considered as the superposition of two harmonic traveling waves which propagate in opposite directions on a semi-infinite conductor (Hagedorn Method) [19]. For a conductor with a single damper, this method leads to suitable results which is accepted as a well-known method and used up until now [22]. Although this approach is extended to the conductors with more than one damper [23], however, as shown in the present study, it does not yield to correct results. Using the conventional method, the damper dissipated power does not considerably change with the increase in the number of dampers [24]. The shortcomings of the given approach originate from the semi-infinite conductor length assumptions in which the boundary conditions cannot take into account. As a result, the eigenvalue problem of the conductor vibration is not solved and the natural frequencies are not obtained. A simple sinusoidal wave is considered as the mode shape, i.e. the phase-amplitude variation of the travelling waves is ignored, and the propagation of waves in the two sides of the span is considered independently.

To overcome the above mentioned problems, the authors of this paper presented a different approach based on energy balance [24]. That is not only considers the effects of the number, location and impedance of the dampers on the vibration mode shape and energy dissipation, but also takes into account the effects of boundary conditions (finite length of the conductor) as well as the travelling wave phase-amplitude variations. The rest of the paper is organized as following: First, mathematical relationships of conductor vibration are presented, and then in section three, the proposed methodology is introduced in more detail. The results of the effect of the damper installation location on vibration amplitude and bending strain, as well as the optimum damper location installation are given in section four, along with the discussion. Finally, the conclusion is given in section five.

2. THE CONDUCTOR VIBRATION

A suitable model for a steady-state vibration of a single conductor with Stock-bridge damper is described in this section.To reach this aim, the governing equations are presented and then EBM is described for solving vibration equation.

2. 1. Equation of Vibration Transmission lines have high tension-to-weight ratio. So the planar vibration equation of the conductor approximated as Equation (1) [14, 15, 19-24].

$$EI\,u^{IV} - Tu'' + \rho\ddot{u} = F_w(x,t) + F_c(u,\dot{u},t) \quad (1)$$

In which EI is the bending stiffness (or flexural rigidity), T is the tensile force, ρ is the mass per unit length, $u(x,t)$ is the vertical displacement, F_w is the wind force (resulting from Karman vortex) and F_c is the conductor internal damping force. The dot sign represents the derivative with respect to time (t) and the prime symbol indicates the derivative with respect to the spatial coordinate (x).

Due to dense frequency spectrum and the occurrence of the lock-in phenomenon in the electric power transmission lines, it is assumed that the steady wind at any speed will induce steady vibration of the conductor at the resonance frequency [14], i.e., the frequency of the steady forced vibration of the conductor will always correspond to one of its natural frequencies and the corresponding mode shape. On the other hand, the bending stiffness and internal damping of the conductor has little influence in determining the natural frequencies and mode shapes of the conductor [19-22, 25-29]. Therefore, the natural frequencies and the corresponding mode shapes of the conductor at any sub-span could be obtained from Equation (2) [19-23].This relation is the taut string free vibration equation and V_c refers to the wave propagation velocity along the string.

$$\ddot{u} = V_c^2 u'' \quad , \quad V_c^2 = \frac{T}{\rho} \quad (2)$$

2. 2. EBM In practical applications, the maximum possible amplitude of conductor vibration is determined by EBM [28]. The amplitude of the steady vibration, in any natural frequency, is to the extent that the input power of aerodynamic forces is equal to the sum of the dissipated powers of the damper and conductor. Therefore, in EBM, the amplitude of the equivalent standing wave (A) at each frequency is obtained from solving the following nonlinear algebraic equation (Equation (3)) [19-23].

$$P_w(A,f) = P_d(A,f) + P_c(A,f) \quad (3)$$

where $f = f_n$ is cable natural frequency; P_w is wind power input, P_d and P_c are dissipated power of damper and conductor respectively.

The power of the wind exerted to a flexible conductor has a complex nature and is subject to various factors such as vibration amplitude and frequency. In order to calculate the maximum amplitude of the vibration, the greatest force of the wind at different frequencies, is experimentally measured. The graphs of the reduced wind power vs. vibration amplitude have been presented in a variety of resources [19-22, 30].

Dissipated energy in the conductor has a number of different sources, and the combination of all types of conductor dissipation is cast into the conductor self-damping effect [14, 15]. The dissipated power of the conductor is measured through the "power", "standing wave" and "decay" methods [31] and its mathematical relations are presented in different references [14, 19-22, 31-33].

The average dissipated power of the Stock-bridge damper (P_d) is calculated through Equation (4).

$$P_d = \frac{1}{2} Z_d \, (\omega A_d)^2 \cos(\theta_z) \tag{4a}$$

$$\omega = 2\pi f \ , \ \bar{Z}_d = Z_d e^{i\theta_z} \tag{4b}$$

where $\bar{Z}_d$ is the complex function of damper impedance that is calculated according to IEC 61897 [34] following the experimental measurement of the exerted force on damper clamp and clamp vibration velocity, and the subscript d is used in the quantities associated with the damper.

It should be noted that the damper amplitude (A_d) is calculated in terms of vibration amplitude (A) by the conductor vibration mode shape which is replaced in Equation (4).

2. 3. The Bending Strain Amplitude After calculating the conductor vibration amplitude, its bending strain amplitude is obtained by Equation (5) [1, 19].

$$\varepsilon(x,t) = \frac{d_i}{2} u''(x,t) \tag{5}$$

The conductor curvature (rate of change in conductor slope) is very high at points such as a crest or clamps, so the fatigue failure occurrence is very high at these locations. Using the perturbation method, the conductor curvature is obtained at discontinuities (crest or clamps) as Equations. (6) and (7) [1, 19]:

$$\varepsilon_1 = \frac{d_i}{2} k^2 A \ , \ k = \frac{2\pi}{\lambda} = \frac{\omega}{V_c} \tag{6}$$

$$\varepsilon_2 = \frac{d_i}{2} \frac{\Delta u'(x,t)}{l_{char}} \ , \ l_{char} = \sqrt{\frac{EI}{T}} \tag{7}$$

where Equation (6) is used for the points located in the "free field" (far from clamp) and Equation (7) is used in the vicinity of the clamp. In the above equations d_i is the conductor characteristic diameter, A is the vibration amplitude, λ is the wavelength, $\Delta u'$ is the change of conductor slope at clamps and l_{char} is the conductor characteristic length.

Equations (6) and (7) show that, the strain amplitude is directly proportional to the characteristic diameter and is inversely proportional to bending stiffness. The actual values of these two parameters are functions of the conductor curvature at some point, and therefore, they depend on time and space [14], which were investigated by some authors [25, 26]. However, since the design is based upon the worst case scenario, the value of the bending stiffness 'EI' is considered to be equal $EI_{\min}$, and the characteristic diameter to be the outer layer conductor strand diameter, [1, 14, 27]. According to the standard reference, the accepted extreme bending strain value of ACSR conductors is 150 microns [4, 27].

3. THE COMPREHANSIVE METHODOLOGY

In this section, an appropriate model is presented for conductorvibration with several dampers. In the proposed approach the eigenvalue problem of the conductor vibration is formed, by taking into account the complex form of the general response of the conductor vibration equation; the solution of which leads to the natural frequencies, damping rates and the complex mode shapes.

3. 1. Eigen Value Problem The general solution for the steady state response of the conductor vibration equation in each sub-spans (Equation (2)), is considered as Equation (8) [24]:

$$u(x,t) = real(\bar{u}(x,t)) \quad , \quad \bar{u}(x,t) = e^{i\omega t} \bar{U}(x) \tag{8a}$$

$$\bar{U}(x) = \bar{A}_0 e^{\gamma x} + \bar{B}_0 e^{-\gamma x} \ , \ \gamma = \frac{s}{V_c} \ , \ s = -\delta + i\omega \tag{8b}$$

$$\bar{A}_0 = A_0 e^{i\theta_A} \quad , \quad \bar{B}_0 = B_0 e^{i\theta_B} \tag{8c}$$

The eigenvalue s is a complex number whose imaginary part is the vibration frequency and the real part is the damping rate. Consequently Equation (8) is transformed to Equation (9):

$$u(x,t) = A_0 e^{-\frac{\delta}{V_c}x} \sin(\omega(t + \frac{x}{V_c}) + \theta_A) + B_0 e^{\frac{\delta}{V_c}x} \sin(\omega(t - \frac{x}{V_c}) + \theta_B) \tag{9}$$

Also, for the Aeolian vibration with small amplitude and slope, the vertical component of conductor tension (q) is written as Equation (10), then Equation (11):

$$q = T \sin(\theta_u) \cong T \tan(\theta_u) = T \frac{du}{dx} \tag{10}$$

$$q(x,t) = real(\bar{q}(x,t)) \tag{11a}$$

$$\bar{q}(x,t) = T \frac{d\bar{u}}{dx} = e^{i\omega t} \bar{Q}(x) \tag{11b}$$

$$\bar{Q}(x) = T\gamma(\bar{A}_0 e^{\gamma x} - \bar{B}_0 e^{-\gamma x}) \tag{11c}$$

Generally, a span which has n_d dampers, will have (n_d+1) sub-spans (Figure 1). Based on this figure, first subspan and last subspan are limited to a support in one end and a damper in other end. However, in the central parts of the conductor, the (p+1)st subspan is located between the pth and (p+1)st dampers and $0 \le x_{p+1} \le l_{p+1}$ (subspan coordinate x_{p+1} is measured from the beginning of the (p+1)st subspan).

In this case, in addition to the s value, there are $2\times(n_d+1)$ complex unknowns ($\bar{A}_0$, $\bar{B}_0$) which are the complex amplitudes of the sub-spans travelling waves. These unknowns can be found by applying the boundary condition at both ends of the span as well as the geometric and force conditions at each damper location.

In each damper location, the force and geometric boundary conditions (Equation (12)) must be satisfied at any time. Where $\bar{F}_d$ is the complex function of damper force.

$$\left\{\begin{array}{l}\left[\bar{u}(x,t)\right]_{x_p=l_p}=\left[\bar{u}(x,t)\right]_{x_{p+1}=0} \quad (12a)\\ \left[\bar{q}\right]_{x_{p+1}=0}-\left[\bar{q}\right]_{x_p=l_p}=\bar{F}_d \quad (12b)\end{array}\right.$$

$$\bar{F}_d = Z_d\cdot\left[\frac{d\,\bar{u}}{dt}\right]_{x_p=0} \quad , \quad p=1,2,3,...,n_d \quad (12c)$$

By applying the values of displacement and force at the beginning of each sub-span ($\bar{U}_0$, $\bar{Q}_0$), the unknown coefficients of the amplitude are obtained in terms of them (Equation (13)):

$$\bar{A}_0=\frac{1}{2}(\bar{U}_0+\frac{1}{T\gamma}\bar{Q}_0) \ , \ \bar{B}_0=\frac{1}{2}(\bar{U}_0-\frac{1}{T\gamma}\bar{Q}_0) \quad (13)$$

So, Equations (8) and (11) are written in the form of Equation (14):

$$\begin{Bmatrix}\bar{U}(x)\\ \bar{Q}(x)\end{Bmatrix}=\begin{bmatrix}\frac{e^{\gamma x}+e^{-\gamma x}}{2} & \frac{1}{T\gamma}\frac{e^{\gamma x}-e^{-\gamma x}}{2}\\ (T\gamma)\frac{e^{\gamma x}-e^{-\gamma x}}{2} & \frac{e^{\gamma x}+e^{-\gamma x}}{2}\end{bmatrix}\begin{Bmatrix}\bar{U}_0\\ \bar{Q}_0\end{Bmatrix}=\begin{bmatrix}\cosh(\gamma x) & \frac{1}{T\gamma}\sinh(\gamma x)\\ (T\gamma)\cdot\sinh(\gamma x) & \cosh(\gamma x)\end{bmatrix}\begin{Bmatrix}\bar{U}_0\\ \bar{Q}_0\end{Bmatrix} \quad (14)$$

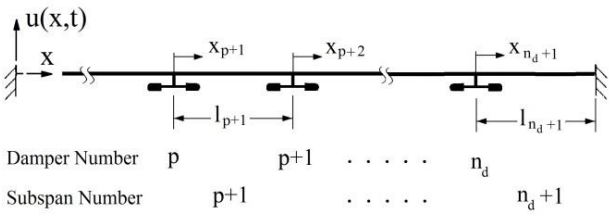

Figure 1. Numbering of dampers and sub-spans

With the aid of the coefficient matrix of the above equation (field matrix), the displacement and vertical force at any point of each sub-span, can be obtained in terms of the values at the beginning of the same sub-span. Equation (12) is also written as Equation (15):

$$\begin{Bmatrix}\bar{U}\\ \bar{Q}\end{Bmatrix}_{x_{p+1}=0}=\begin{bmatrix}1 & 0\\ (i\omega)\bar{Z} & 1\end{bmatrix}\begin{Bmatrix}\bar{U}\\ \bar{Q}\end{Bmatrix}_{x_p=l_p} \quad (15)$$

By the coefficient matrix of the above equation (Point matrix), the displacement and vertical force at the beginning of the sub-span can be obtained in terms of the corresponding values at the end of the previous sub-span.

Thus, using the transfer matrix method and chain multiplication of the field matrix (for any sub span) and the point matrix (for any damper) [34, 35], we come to the following linear equation system (Equation (16)), which relates the displacement and the vertical force at the beginning and the end of the entire span.

$$\begin{Bmatrix}U\\ Q\end{Bmatrix}_{x=L}=\begin{bmatrix}D_{11} & D_{12}\\ D_{21} & D_{22}\end{bmatrix}\begin{Bmatrix}U\\ Q\end{Bmatrix}_{x=0} \quad (16)$$

The matrix D is obtained from the chain multiplication of field and point matrices, and its entries are nonlinear functions of variable s and include parameters of damper impedance, the lengths of sub-spans, tension and mass per unit length of the conductor. The boundary conditions at both conductor ends are written as Equation (17):

$$\bar{u}(x_1=0\ ,\ t)=\bar{u}(x_{n_d+1}=l_{n_d+1}\ ,\ t)=0 \quad (17)$$

Appling Equation (17) to Equation (16) results in Equation (18):

$$D_{12}(s)\cdot Q_{x=0}=0 \quad (18)$$

Given that, the vertical force component at the beginning of the span ($Q_{x=0}$), in general, is nonzero, finally the characteristic equation is achieved as Equation (19):

$$D_{12}(s)=0 \quad (19)$$

By solving this nonlinear equation, eigenvalues (including natural frequencies and relevant damping rates) are extracted. Then, for each eigenvalue, the amplitude coefficients of the sub-spans ($\bar{A}_0$, $\bar{B}_0$) are calculated using Equation (13), in terms of the force at the beginning of the span ($Q_{x=0}$), and the complex mode shape of each sub-span ($\bar{U}(x)$) is obtained.

For a conductor without damper, the new approach is adapted to the classic approach. In this case, the characteristic equation (Equation (19)) leads to the standing wave and completely imaginary eigenvalues:

$$\sinh(\gamma L)=0 \tag{20}$$

$$s=\pm i\omega \ , \ \omega=n\frac{\pi V_c}{L} \ , \ n=0,1,2,... \tag{21}$$

$$u(x,t)=A\sin(kx)\sin(\omega t+\theta) \ , \ k=\frac{\omega}{V_c} \tag{22}$$

3. 2. Equivalent Standing Wave Amplitude In the literatures the input power of the wind (P_w) and dissipated power of the conductor (P_d), are presented in terms of a single value (A) which is the harmonic standing wave amplitude, while in the conductor with damper(s), waves travel along the span and exchange energy between the sub-spans getting different amplitude at each sub-span. So extracting equivalent standing wave amplitude is necessary for obtaining damper dissipated power and applying the EBM. Since, the local wind power input along a conductor depends on the local displacement amplitude [14, 15], the equivalent standing wave amplitude can be defined as the mean amplitude of the vibration along the span, over a period (Equation 23).

$$\begin{aligned} A&=\frac{\frac{1}{\tau\cdot L}\int_0^{\tau}(\sum_{n=1}^{n=n_d}(\int_0^{l_n}|u(x,t)|dx)\,dt)}{\frac{1}{\tau\cdot\lambda}\int_0^{\tau}(\int_0^{\lambda}|\sin(kx)\sin(\omega t)|dx)dt} \\ &=(\frac{2}{\pi})^2\frac{1}{\tau\cdot L}\int_0^{\tau}(\sum_{p=1}^{p=n_d}(\int_0^{l_p}|u(x_p,t)|dx_p)\,dt) \end{aligned} \tag{23}$$

By extracting the equivalent amplitude and normalizing the complex mode shape, dissipated energy of each damper (Equation (4)), is obtained in terms of the of equivalent standing wave amplitude. Then, by establishing the energy balance, the actual amplitude of the conductor vibration is calculated at each natural frequency. Next, by calculating the maximum change in the slope of the conductor, the maximum amplitude of bending strain is calculated at critical points through Equations (6) and (7).

It is worth mentioning that, in extracting the roots of the nonlinear characteristic equation the iterative method is employed. The initial guesses for the roots are the damper-free conductor natural frequencies, and the iteration is terminated when the value of the characteristic equation is less than 10^{-15}. In the iteration process the damper impedance should be available as a function of frequency. For this purpose, the results of the experimental data are used to estimate the mathematical model. Figure 2 shows the conformity of the experimental results, to the estimated model. Experimental results are obtained from Stock-bridge damper impedance test which is performed in the Vibration Research Laboratory, University of Tabriz.

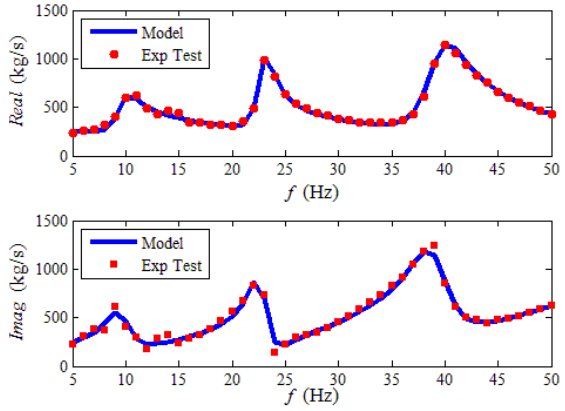

Figure 2. Conformity of the experimental results and theoretical model of Damper Impedance

4. RESULTS AND DISCUTION

Given the importance of the optimal range of damper installation point, the effect of the installation location of the damper is investigated for a transmission line with one damper and with the geometric and physical properties listed in Table 1.

A line with one damper has two sub-spans (side sub-span and main sub-span). Defining some quantities as following, will facilitate presenting the obtained results:

The "node frequency", "dimensionless distance" of the damper installation pointand "dimensionless frequency" are defined as Equation (24) to Equation (26), respectively.

$$f_{node}=n\frac{\sqrt{T/\rho}}{2x_d} \ , \ n=1,2,3,... \tag{24}$$

$$\phi=\frac{x_d}{0.5\lambda_{\min}} \tag{25}$$

$$\mu=\frac{f}{f_{\max}} \tag{26}$$

Where $\lambda_{\min}$ and $f_{\max}$ are the minimum wavelength and the max. Frequency at the intended frequency interval. For power line with the above mentioned properties (Table 1), the minimum wavelength is equal to 3.6 m.

TABLE 1. Conductor properties

Cable Type	D (mm)	ρ (kg/m)	T (kN)	EI (Nm^2)	L (m)
ACSR	31	1.63	37	25	300

The damper relative amplitude (A_{rel}^{d}), the ratio of the damper amplitude to the maximum amplitude of the side sub-span (A_{s}^{d}) and the ratio of the maximum amplitude of the side sub-span to the maximum amplitude of the main sub-span (A_{s}^{s}) are defined as Equation (27).

$$A_{rel}^{d}=\frac{A_d}{A}\ ,\ A_{s}^{d}=\frac{A_d}{(A_{\max})_{sub}}\ ,\ A_{s}^{s}=\frac{(A_{\max})_{sub}}{(A_{\max})_{span}} \quad (27)$$

4. 1. The Effect of Damper Location on Eigenvalues Changes in the real part of eigenvalues (damping rate) with respect to the location of a damper in the range of $0<\phi<1$ are shown in Figure 3. According to this figure, as the distance of the installation point increases, the peaks of the graphs become wider, and are displaced to the left direction. This diagram shows that by increasing the ϕ the mean damping rate increases at the lower half frequency band ($0<\mu<0.5$) and decrease at higher half ($0.5<\mu<1$). Based on this figure, the critical frequency area with low damping rate, can be distinguished.

4. 2. Effect of Damper Location on Damper Amplitude Changes in the damper relative amplitude with respect to the increase in the distance of the installation location are shown in Figure 4.

As long as $\phi<1$, the relative amplitude A_{rel}^{d} is not equal zero at any frequency, but when $\phi=1$ the displacement of the damper at the end of the frequency range (about 42 Hz), is very close to zero, that is to say the damper is placed on the node. When ϕ is an integer, the length of the side sub-span is equal to an integer multiple of the wavelength-half (loop length). At this time, the location of the damper at some frequencies which defined as node frequencies coincides with the node, the damper efficiency becomes zero and the vibration shape of the conductor in the entire sub-span, turns into a standing wave. According to this figure, installing the damper at distances greater than the shortest loop length($\phi>1$), causes the displacement of the damper severely decrease at "node frequencies".

The locus of “node frequencies” (Equation 24) on "frequency-installation point" plane, is a set of curves, in whose vicinity, the displacement amplitude of the damper is very small. Figure 5 shows the contours of the A_{s}^{d} where the dark areas are node frequency zones for the $n=1, 2$. According to Figure 5, before reaching the first node frequency curve, A_{s}^{d} is equal to one, i.e. the damper point has the greatest amplitude in the side sub-span. But when it reaches this range, the location of the damper is converted into a node, and this ratio sharply decreases. Also, after this range, this ratio rapidly changes between zero and one.

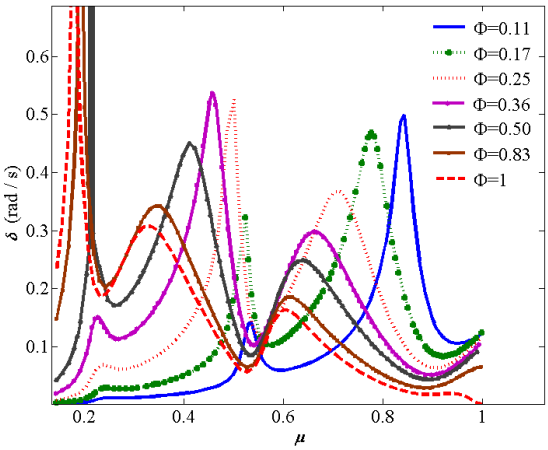

Figure 3. Changes in the dampeing rate of eigenvalues with respect to damper location

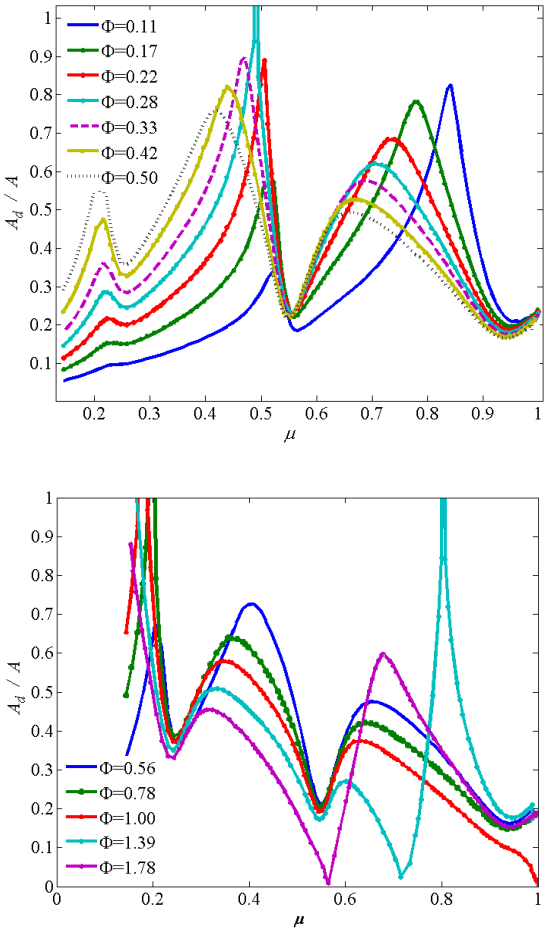

Figure 4. Changes in the damper relative amplitude with respect to installation location

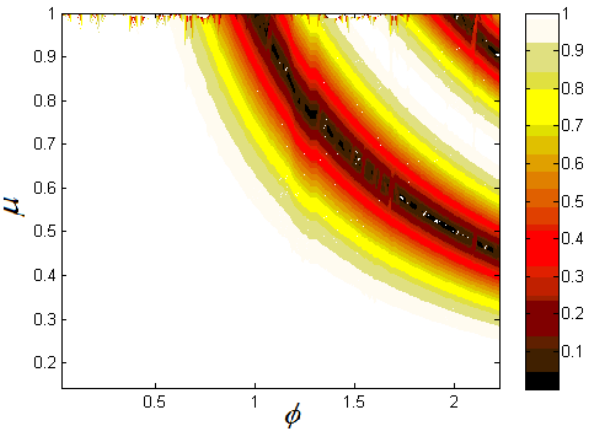

Figure 5. Changes in the ratio of the damper amplitude to the maximum amplitude of the side sub-span (A_s^d)

Figure 6 shows the contours of the A_s^s with respect to the frequency and installation point for $0 \le A_s^s \le 1$. In the dark area A_s^s is higher than one, while outside this zone, this ratio is always less than one. Based on Figure 5 the dark area is the first node frequency range. According to Figure 6, when the damper coincides with the node, the amplitude of the side sub-span peak becomes greater than the amplitude of the main sub-span peak, and the side sub-span vibrates more severely. Comparison between Figures 5, 6 and 3 showed that before reaching the first node frequency, the ratio of the damper amplitude to the maximum amplitude of the span is always less than one and decreases sharply in critical frequencies (frequencies with low damping rate).

4. 3. Effect of Damper Point on Conductor Vibration Amplitude The effect of the damper location on the conductor vibration amplitude is shown in Figure 7. Figures 7a and 7b devoted to $0 < \phi < 1$ and Figure 7c is covering the $1 < \phi$ range.

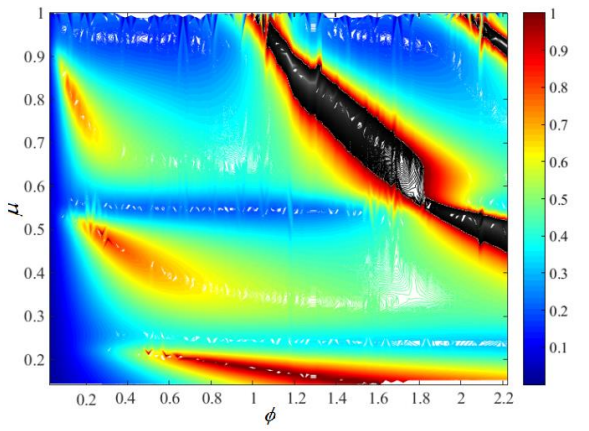

Figure 6. Changes in the ratio of the side sub-span maximum amplitude to the main sub-span maximum amplitude (A_s^s). In the dark area A_s^s is higher than one.

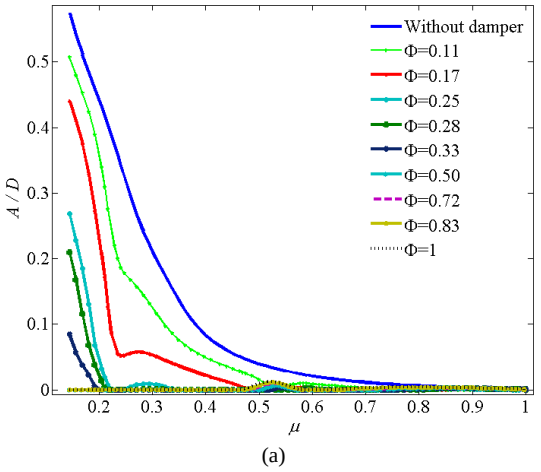

(a)

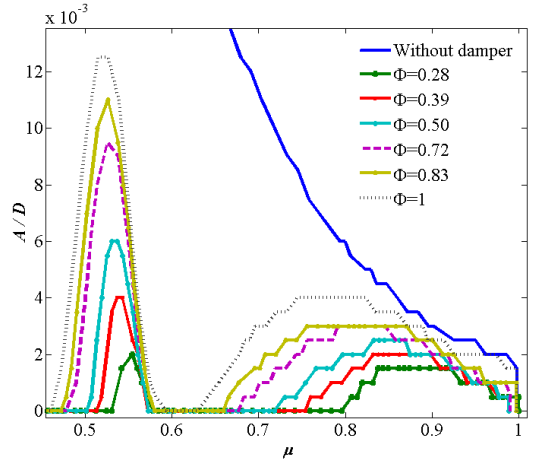

(b)

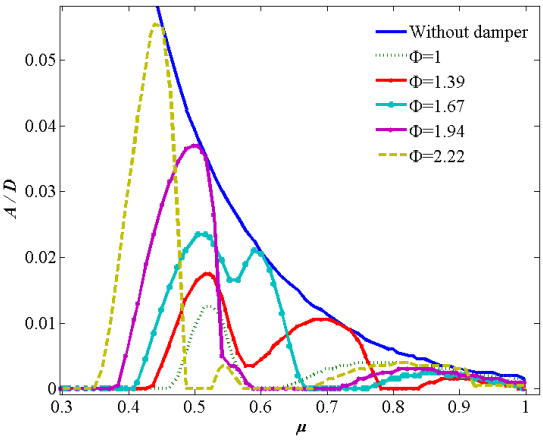

(c)

Figure 7. The effect of the damper location on the conductor vibration amplitude for (a) $\phi < 1$, (b) $\phi < 1$ (at higher frequencies) and (c) $\phi > 1$

In general, for each installation point, as frequency increases, the vibration amplitude decreases. According to the Figure 7a, at lower half frequency range, as the damper moves away from the support, the vibration amplitude of the conductor sharply decreases, i.e. as the distance between the installation location and support (x_d) increases, the efficiency of the damper increases. Because for a given frequency, as the x_d increases from zero, the damper location displaces from the node towards the peak, and the relative displacement of the damper and thus its dissipated power increases.

The further investigations show that when $\phi > 0.3$ at a wide range of frequencies, the steady vibration amplitude is almost zero. Figure 7b is the frequency zoomed of Figure 7a. Comparing this figure with Figure 7a, shows that increasing the x_d reduces the conductor vibration amplitude of lower half frequency; but the continuation of this process, strongly increases the vibration amplitude at higher half frequencies.

According to Figure7c, which the damper has been installed at distances greater than the shortest loop length, although the vibration amplitude of the conductor is zero at lower half frequencies, but the vibration amplitude of the conductor increases at higher half frequency, and becomes tangent to the graph of vibration amplitude of damper-free conductor, in the vicinity of relevant node frequencies. Therefore, the optimal location for installing the first damper on a span is calculated through minimizing the mean vibration amplitude along the span. For the presented physical and geometric characteristics, the optimal installation point is $0.4 < \phi < 0.7$ ($0.75 < x_d < 1$ meters).

4. 4. Bending Strain Drawing the graph of bending strains at critical points shows that, in the case that only one damper is installed along the span in $\phi < 1$ the bending strain has the maximum amplitude, in the vicinity of the supports, the damper location and free field, respectively, and the strain in the clamp of a support close to the damper, is a little greater than the strain in the clamp of a support which is farther away from the damper. According to the results obtained, the bending strain near the support is almost a hundred times greater than the bending strain in the free field (Figure 8). Of course, in practical situations, by taking into account the effect of bending stiffness on the mode shapes, and taking the length of the damper clamp into consideration, this difference will decrease. However, this result indicates that calculating the strain is more important in the location of clamps, than in the free field. Calculating the optimal installation location, based on the minimum mean strain in clamps, confirms the optimal value obtained in the previous section.

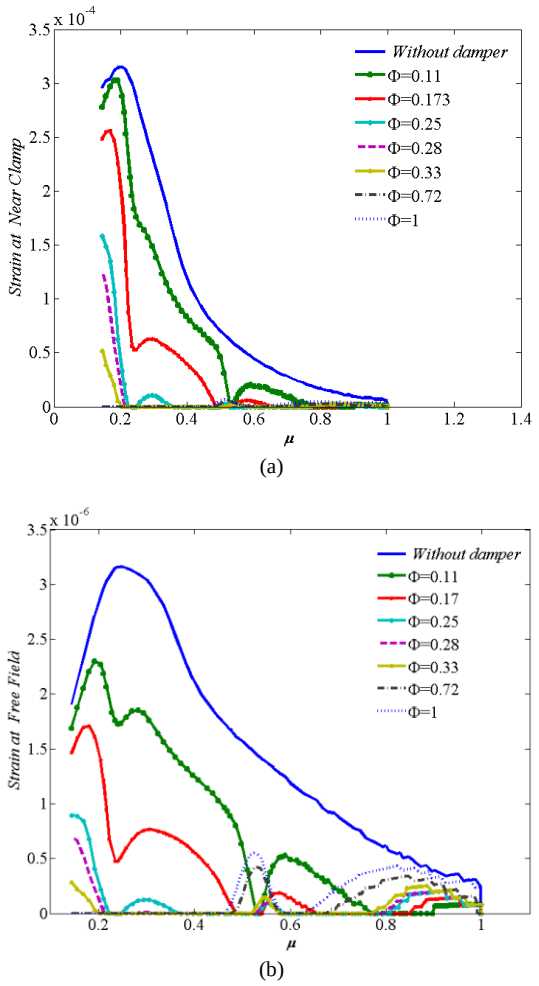

Figure 8. The bending strain a) at support close to the damper b) at free field

5. CONCLUSION

In the present study, a model is presented for transmission lines with more than one damper, which can consider the effects of traveling of the wave, damper location, damper impedance and the phase-amplitude fluctuations along the span, on the vibration mode shape and damper dissipated power. Thus, a more accurate result will be obtained for the vibration amplitude of the conductor, with the EBM. In the methods presented earlier, above factors were being ignored, and the conductor vibration amplitude was being calculated based on simplifying assumptions whose incorrectness revealed by new method results.

The outcomes obtained from this research, while confirming the standing waveform in the damper-less state, show that in the presence of dampers, waves in inner sub-spans are traveling and wave propagation is towards dampers. Also, the vibration amplitude is variable along the conductor, and the movement of

points on a conductor is associated with phase difference.

Solving the eigenvalue problem for each installation location shows that the real part of the eigenvalues, which was ignored in other methods, is a very important parameter, and with its help, critical frequency ranges (with high vibration potential) can be identified. So, with this new method there is no need to calculate the vibration amplitude. According to the obtained results, the real part of the eigenvalues depend on the damper installation location, and it increases at low frequencies, as the damper installation distance increases from zero.

This study shows that the dissipated energy, vibration amplitude and bending strain, greatly depend on the damper installation location, and it is necessary to calculate the optimal installation location for each certain condition. The present research showed that, as the distance between the damper installation location and the support increases, the damper efficiency increases (especially at low frequencies), but the continuation of this process, results in the reduction of the damper efficiency at higher frequencies, and the optimal range for damper location is obtained through this procedure. Installing a damper in the optimal range increases the damping rates. Installing the damper, at a distance greater than the shortest loop length, while reducing the efficiency of the damper, causes the amplitude of the side sub-span to become much larger than that of the main sub-span.

Calculation of the bending strain along the span shows that the bending strain has greater values in the clamps. In the case that only one damper is installed along the span at a distance less than the shortest wavelength, the bending strain has the maximum value in the "support close to the damper", "support farther away from the damper", "damper clamp" and "free field", respectively, and the bending strain in the near damper support clamp is almost a hundred times greater than the bending strain in the free field and therefore the calculation of the strain in the location of the clamps, is more important than in the free field.

6. REFERENCES

1. Kiessling, F., Nefzger, P., Nolasco, J., and Kaintzyk, U., Overhead power lines: planning, design, construction, Springer Science & Business Media, (2014).
2. Chan, J., Havard, D., Rawlins, C., Diana, G., and Cloutier, L., EPRI Transmission Line Reference Book: wind-induced Conductor Motion, Electric Power Research Institute (EPRI), (2009).
3. Bayliss, C., Bayliss, C., and Hardy, B., Transmission and distribution electrical engineering, Elsevier, (2012).
4. Hartmann, G.K.D., and Kern, G.G., Wind Induced Vibrations on High Voltage Overhead Lines, Mosdorfer, Austria, (1994).
5. Emamgholizadeh, M.J., Gharabaghi, A.M., Abedi, K., and Sedaaghi, M., "Experimental investigation of the effect of splitter plate angle on the under-scouring of submarine pipeline due to steady current and clear water condition", ***International Journal of Engineering-Transactions C: Aspects***, Vol. 28, No. 3, (2014), 368–377.
6. Dulhunty, P., "Vibration dampers on AAC and AAAC conductors", In 22nd International Conference and Exhibition on Electricity Distribution (CIRED 2013), Institution of Engineering and Technology, Stockholm, (2013), 1–4.
7. Liu, S., Sun, N., Yin, Q., Qi, Y., Cao, D., and Zhang, L., "Study of New Vibration Suppression Devices for Application to EHV Transmission Line Groundwires", ***Energy Procedia***, Vol. 12, (2011), 313–319.
8. Krispin, H.J., Fuchs, S., and Hagedorn, P., "Optimization of the Efficiency of Aeolian Vibration Dampers", In IEEE Power Engineering Society Conference and Exposition in Africa - PowerAfrica, IEEE, (2007), 1–3.
9. Varney, T., "Notes on the vibration of transmission-line conductors", ***Journal of the American Institute of Electrical Engineers (AIEE)***, Vol. 45, No. 10, (1926), 953–957.
10. Claren, R., and Diana, G., "Mathematical Analysis of Transmission Line Vibration", ***IEEE Transactions on Power Apparatus and Systems***, Vol. PAS-88, No. 12, (1969), 1741–1771.
11. Dhotarad, M.S., Ganesan, N., and Rao, B.V.A., "Transmission line vibrations", ***Journal of Sound and Vibration***, Vol. 60, No. 2, (1978), 217–237.
12. Li L., De-yi K., Xiao-hong L., and Zheng-ping L., "Analysis of Aeolian Transmission Conductor with Dampers by the Finite Element Method", ***High Voltage Engineering***, Vol. 34, No. 2, (2008), 324–328.
13. Li, L., De-Yi, K., Xiao-Hong, L., and Zheng-ping, L., "Numerical simulation of aeolian vibrations transmission lines by CFD", ***Engineering Mechanics***, Vol. 26, No. S2, (2009), 235–240.
14. Vecchiarelli, J., "Aeolian vibration of a conductor with a Stockbridge-type damper", Doctoral dissertation, University of Toronto, (1998).
15. Vecchiarelli, J., Currie, I.G., and Havard, D.G., "Computational analysis of aeolian conductor vibration with a stockbridge-type damper", ***Journal of Fluids and Structures***, Vol. 14, No. 4, (2000), 489–509.
16. Langlois, S., and Legeron, F., "Prediction of Aeolian Vibration on Transmission-Line Conductors Using a Nonlinear Time History Model—Part I: Damper Model", ***IEEE Transactions on Power Delivery***, Vol. 29, No. 3, (2014), 1168–1175.
17. Guerard, S., Godard, B., and Lilien, J.L., "Aeolian Vibrations on Power-Line Conductors, Evaluation of Actual Self Damping", ***IEEE Transactions on Power Delivery***, Vol. 26, No. 4, (2011), 2118–2122.
18. Godard, B., Guerard, S., and Lilien, J.L., "Original Real-Time Observations of Aeolian Vibrations on Power-Line Conductors", ***IEEE Transactions on Power Delivery***, Vol. 26, No. 4, (2011), 2111–2117.
19. Hagedorn, P., "Ein einfaches Rechenmodell zur Berechnung winderregter Schwingungen an Hochspannungsleitungen mit Dampfern", ***Ingenieur-Archiv***, Vol. 49, No. 3–4, (1980), 161–177.
20. Hagedorn, P., "On the computation of damped wind-excited vibrations of overhead transmission lines", ***Journal of Sound and Vibration***, Vol. 83, No. 2, (1982), 253–271.
21. Wolf, H., Adum, B., Semenski, D., and Pustaić, D., "Using the Energy Balance Method in the Estimation of Overhead Transmission Line Aeolian Vibrations", ***Strojarstvo***, Vol. 50, No. 5, (2008), 269–276.
22. Kasap, H., "Investigation of Stockbridge dampers for vibration

control of overhead transmission lines", Doctoral dissertation, Middle East Technical University, (2012).

23. Sadeghi, S.M., and Rezaei, A., "Extending of 'Energy Balance Method' for Calculating of Cable Vibration with Arbitrary Number of Dampers and their Optimal Placement", ***Modares Mechanical Engineering***, Vol. 15, No. 8, (2015), 438–448.
24. Rezaei, A., and Sadeghi, M.H., "Aeolian Vibrations of Transmission Line Conductors with More than One Damper", ***International Journal of Engineering-Transactions A: Basics***, Vol. 28, No. 10, (2015), 1515–1524.
25. Langlois, S., Legeron, F., and Levesque, F., "Time History Modeling of Vibrations on Overhead Conductors With Variable Bending Stiffness", ***IEEE Transactions on Power Delivery***, Vol. 29, No. 2, (2014), 607–614.
26. Levesque, F., Goudreau, S., Langlois, S., and Legeron, F., "Experimental Study of Dynamic Bending Stiffness of ACSR Overhead Conductors", ***IEEE Transactions on Power Delivery***, Vol. 30, No. 5, (2015), 2252–2259.
27. Braga, G.E., Nakamura, R., and Furtado, T.A., "Aeolian vibration of overhead transmission line cables: endurance limits", In IEEE/PES Transmision and Distribution Conference and Exposition: Latin America, IEEE, (2004), 487–492.
28. Kraus, M., and Hagedorn, P., "Aeolian vibrations: wind energy input evaluated from measurements on an energized transmission line", ***IEEE Transactions on Power Delivery***, Vol. 6, No. 3, (1991), 1264–1270.
29. Hagedorn, P., "Wind-excited vibrations of transmission lines: A comparison of different mathematical models", ***Mathematical Modelling***, Vol. 8, (1987), 352–358.
30. Diana, G., and Falco, M., "On the forces transmitted to a vibrating cylinder by a blowing fluid", ***Meccanica***, Vol. 6, No. 1, (1971), 9–22.
31. IEEE Standards, "IEEE Std. 563- IEEE Guide on Conductor Self Damping Measurements", IEEE Power & Energy Society, New York, U. S. A., (1978).
32. Guérard, S., "Power line conductors, a contribution to the analysis of their dynamic behaviour", Doctoral dissertation, Université de Liège, Belgique, (2011).
33. Noiseux, D.U., "Similarity laws of the internal damping of stranded cables in transverse vibrations", In Proceedings of the 1991 IEEE Power Engineering Society Transmission and Distribution Conference, IEEE, 817–823.
34. IEC Standards, "IEC Std 61897- Requirements and tests for Stockbridge type Aeolian vibration dampers", International Electro technical Commission, Switzerland, (1998).
35. Dimarogonas, A.D., Vibration for Engineers, Prentice Hall, (1996).

Analysis of Aeolian Vibrations of Transmission Line Conductors and Extraction of Damper Optimal Placement with a Comprehensive Methodology

A. Rezaei, M. H. Sadeghi

Department of Mechanical Engineering, University of Tabriz, Tabriz, Iran

P A P E R I N F O

Paper history:
Received 26 February 2018
Received in revised form 20 April 2018
Accepted 26 April 2018

Keywords:
Aeolian Vibration
Transmission Line
Energy Balance Method
Stock-bridge Damper
Optimum Location

چکیده

تعیین دامنه ارتعاشات «آولین» رساناهای خطوط انتقال برق دارای میراگر «استاک‌بریج»، به دلیل پیچیدگی رفتار رسانای رشته‌ای، از روش «تعادل انرژی» انجام می‌شود. دقت نتایج بدست آمده از این روش، به شدت به شکل مود فرض شده برای ارتعاش رسانا وابسته است. در تحقیق حاضر با در نظر گرفتن یک مدل مناسب برای ارتعاش رسانا، روش جامعی برای محاسبه‌ی دامنه ارتعاش پایای رسانای دارای تعداد دلخواه میراگر ارایه می‌شود. در این روش، اثرات روندگی موج، تغییر دامنه و فاز نسبت به زمان، شرایط مرزی دو انتها (طول محدود رسانا) و همچنین تاثیر تعداد، محل نصب و امپدانس میراگر در شکل مود ارتعاشی لحاظ می‌شود و فرکانس‌های طبیعی، نرخ میرایی و شکل مودهای مختلط از تشکیل و حل مساله مقدار ویژه غیرخطی مربوطه بدست آورده می‌شود. همچنین با استفاده از این روش اثر محل نصب میراگر بر روی دامنه ارتعاش و کرنش خمشی رسانا بررسی شده و محل نصب بهینه استخراج می‌شود. مقادیر بدست آمده نشان می‌دهند در نظر گرفتن پارامترهای فوق اثر قابل ملاحظه‌ای بر دقت نتایج دارد.

***doi**: 10.5829/ije.2019.32.02b.19*